

Structural Basis of Specific Binding between Aurora A and TPX2 by Molecular Dynamics Simulations

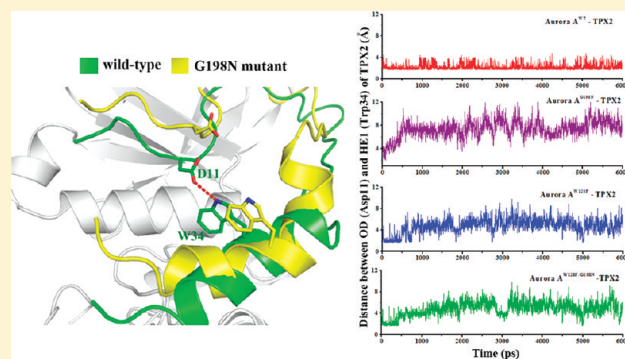
Yuanhua Cheng^{†,‡}, Fushi Zhang[†], Quan Chen[‡], Jian Gao[‡], Wei Cui[‡], Mingjuan Ji^{*,‡}, and Chen-Ho Tung^{*,†}

[†]Key Laboratory of Organic Optoelectronics and Molecular Engineering of Ministry of Education, Department of Chemistry, Tsinghua University, Beijing 100084, P.R. China

[‡]College of Chemistry and Chemical Engineering, Graduate University of Chinese Academy of Sciences, Beijing 100049, P.R. China

Supporting Information

ABSTRACT: In the present study, the impacts of G198N and W128F mutations on the recognition between Aurora A and targeting protein of *Xenopus* kinesin-like protein 2 (TPX2) were investigated using molecular dynamics (MD) simulations, free energy calculations, and free energy decomposition analysis. The predicted binding free energy of the wild-type complex is more favorable than those of three mutants, indicating that both single and double mutations are unfavorable for the Aurora A and TPX2 binding. It is also observed that the mutations alternate the binding pattern between Aurora A and TPX2, especially the downstream of TPX2. An intramolecular hydrogen bond between the atom OD of Asp¹¹^{TPX2} and the atom HE1 of Trp³⁴^{TPX2} disappear in three mutants and thus lead to the instability of the secondary structure of TPX2. The combination of different molecular modeling techniques is an efficient way to understand how mutation has impacts on the protein–protein binding and our work gives valuable information for the future design of specific peptide inhibitors for Aurora A.



INTRODUCTION

Aurora kinases represent a highly conserved family of serine/threonine kinases that have been identified as pivotal regulators of the mitotic cell division process.^{1,2} Mammals express three Aurora kinase paralogues, Aurora A, Aurora B, and the less well characterized Aurora C.³ Aurora kinases consist of a N-terminal regulatory domain and a C-terminal catalytic domain.⁴ Aurora A and Aurora B, which share 70% sequence homology in their catalytic domains, are distinct in subcellular localization and functions.^{5–8} As a key regulator, Aurora A localizes to the spindle pore and the microtubule, and it is essential for many mitotic events including mitotic entry, centrosome maturation and separation, spindle assembly, and cytokinesis.^{8–10} Overexpression of Aurora A results in centrosome amplification, aneuploidy, chromosomal instability, and extended telomeres, which are the characteristic hallmarks of cancer.^{10–12} Aurora B is implicated in chromosomal alignment and separation and has also been identified to play a key role in the tension sensing machinery of the spindle checkpoint as well as targeting checkpoint proteins to the kinetochores in anaphase onset and the cytokinesis.^{13–16}

Despite the great similarity of their sequence and structure, both of them are tightly regulated by their specific partner proteins in mitosis. During mitosis, a microtubule-associated component, the targeting protein of *Xenopus* kinesin-like protein 2 (TPX2), has been identified to be a crucial binding partner to

anchor Aurora A to spindle microtubules.^{17,18} Besides, as an allosteric activator, TPX2 binding pulls on the activation segment of Aurora A to swing the phosphothreonine into a buried position and lock Aurora A in the active conformation as well as enhance its autophosphorylation by preventing the dephosphorylation of activation segment from protein phosphatase 1 (PP1).^{19–21} Another microtubule-binding protein, the von Hippel-Lindau protein (pVHL), has been shown to bind strongly to the TPX2 binding region of Aurora A and may be involved in the degradation pathway of Aurora A via the E3 ubiquitin ligase complex.²² On the contrary, the localization of Aurora B is associated with an intact chromosomal passenger complex containing at least three other proteins, INCENP, Survivin, and Borealin.^{23–28}

Recently, the crystal structure of Aurora A complexed with TPX2 was determined at the atomic level by X-ray diffraction method.¹⁹ It is reported that TPX2 binds to Aurora A with two separate stretches (residues 7–21 and residues 30–43) recognized at two distinct sites.¹⁹ Besides, the basis for the interactions between Aurora A or Aurora B with its specific partner proteins also arouse great interest. Some studies demonstrated that one single amino acid difference (G198 for Aurora A and N142 for Aurora B)

Received: June 1, 2011

Published: September 15, 2011

might be responsible for the binding specificity of TPX2 between Aurora A and Aurora B.^{29–31} The result of immunoprecipitation indicates that the mimic of Aurora B (Aurora A^{G198N}) bound less TPX2 than the wild-type Aurora A (Aurora A^{WT}).³¹ Meanwhile, the region surrounding this amino acid is almost the same for Aurora A and Aurora B, except for the residues G198/W128 and N142/F72 in Aurora A and Aurora B, respectively.³⁰ Considering the F appears along with N in Aurora B, whereas W is always found covariant with G in Aurora A, the difference of this residue might also influence the binding between Aurora A and TPX2.

Discussing how these two amino acids mutation influence the binding between Aurora A and TPX2 could be valuable for us to understand the binding mechanism and further provide some clues for the design of specific peptide inhibitors of Aurora A. For this purpose, three mimics of Aurora B (Aurora A^{G198N}, Aurora A^{W128F}, and Aurora A^{G198N/W128F}) were constructed based on the wild-type model by mutating the targeting residues to the desired amino acids. Additionally, molecular dynamics (MD) simulations, Molecular Mechanics/Poisson–Boltzmann Surface Area (MM/PBSA) free energy calculations,^{32–45} and Molecular Mechanics/Generalized Born Surface Area (MM/GBSA) free energy decomposition analysis were conducted in this work.^{46–49} The predicted binding free energies and structures of four models were carefully compared to understand how one or two amino acid difference leads to the variant binding affinities between Aurora A and TPX2. Our investigation uncovers an intramolecular hydrogen bond between Asp11^{TPX2} and Trp34^{TPX2}, which is crucial for the stability of TPX2, disappear in the three mutants. We expect that this work would provide the molecular mechanism of how single mutation has impacts on the protein–protein interaction, and our work gives valuable information for the future design of specific peptide inhibitors for Aurora A.

MATERIALS AND METHODS

The Initial Structure. The WT model of ternary Aurora A/TPX2/ATP complex was constructed based on the crystal structure of Aurora A/TPX2 complex (PDB entry: 1OL5¹⁹) and Aurora A/AMPPNP complex (PDB entry: 2DWB⁵⁰), which were retrieved from the RCSB Brookhaven Protein Data Bank (PDB).⁵⁰ The crystal structure of Aurora A/AMPPNP complex was superimposed onto the structure of Aurora A/TPX2 complex, and the AMPPMP was extracted and merged into the Aurora A/TPX2 complex. Then, AMPPNP was modified to mimic ATP. Two Mg²⁺ ions occupy a primary site that chelates β and γ phosphates and a secondary site that chelates α and γ phosphates. The missing residues of TPX2 (residues 22–29) were modeled by the *biopolymer* module in SYBYL7.1. This constructed structure of WT model was immersed in a truncated octahedron box with TIP3P water molecules and minimized by the *sander* program via two steps: first, the water molecules and the added residues were minimized by restraining the protein (5000 cycles of steepest descent and 5000 cycles of conjugate gradient minimizations); second, the whole system was minimized without any restraint (5000 cycles of steepest descent and 5000 cycles of conjugate gradient minimizations). After minimization, the water molecules were deleted by SYBYL7.1, and the final structure of WT model was saved. Three mutants were constructed based on the final WT model by mutating the targeting residues into the desired amino acids. The missing hydrogen atoms of each model were added via the *t leap* program in AMBER9.0.⁵¹

In the following molecular mechanics (MM) minimizations and MD simulations, the AMBER03 force field was used to establish the potentials of the proteins.⁵² The force field parameters of phosphorylated threonine⁵³ (T2P) residues as well as ATP⁵⁴ were downloaded from the AMBER parameter database. In order to neutralize the charge of the complex, counterions of Na⁺ ions were placed on the grids with the largest negative Coulombic potentials around the protein. Then, the whole system was immersed with TIP3P water molecules in a truncated octahedron box, which extended 12 Å away from any solute atoms.⁵⁵

MD Simulations. Precede the MD simulations, the *sander* program was applied to minimize the structure via three steps: first, the water molecules/ions were minimized by restraining the protein (4000 cycles of steepest descent and 2000 cycles of conjugate gradient minimizations); second, the side chains of the protein were minimized by restricting the backbone of the protein (5000 cycles of steepest descent and 2500 cycles of conjugate gradient minimizations); finally, the whole system was minimized without any restraint (10000 cycles of steepest descent and 5000 cycles of conjugate gradient minimizations).

In the MD simulations, Particle Mesh Ewald (PME) was employed to calculate the long-range electrostatic interactions.⁵⁶ The SHAKE procedure was applied, and the time step was set to 2.0 fs.⁵⁷ The systems were gradually heated in the NVT ensemble from 0 to 310 K over 60 ps. Then, 6 ns MD simulations were performed under the constant temperature of 310 K. During the sampling process, the coordinates were saved every 0.2 ps, and the conformations generated from the simulations were used for further binding free energy calculations and decomposition analysis.

MM/PBSA Calculations. The binding free energy of each system was calculated using MM/PBSA technique according to the following equation³⁵

$$\begin{aligned}\Delta G_{\text{bind}} &= G_{\text{complex}} - G_{\text{protein}} - G_{\text{ligand}} \\ &= \Delta E_{\text{MM}} + \Delta G_{\text{PB}} + \Delta G_{\text{SA}} - T\Delta S\end{aligned}\quad (1)$$

where ΔE_{MM} is the MM interaction energy between the receptor and the ligand; ΔG_{PB} and ΔG_{SA} are the polar and nonpolar contributions to desolvation upon ligand binding, respectively; and $-T\Delta S$ is the conformation entropic contribution at temperature T .

Here, the polar desolvation energy was calculated by solving the Poisson–Boltzmann (PB) equations.⁵⁸ In the PB calculations, the grid size used to solve the Poisson–Boltzmann equation was 0.5 Å, and the values of solvent dielectric constant and solute dielectric constant were set to 80 and 1, respectively. The nonpolar contribution was estimated to be proportional to the solvent accessible surface area (SASA) which are determined using the Laboratoire de Chimie des Polymères Organiques (LCPO) method with a solvent-probe radius of 1.4 Å: $\Delta G_{\text{SA}} = 0.0072 \times \Delta \text{SASA}$.⁵⁹ The calculations for the binding free energy were accomplished by using the *mm_pbsa* program in AMBER 9.0. The normal-mode analysis was performed to estimate the change of the conformational entropy upon the ligand binding ($-T\Delta S$) via the *nmode* program in AMBER9.0.⁵¹ The protein–protein binding free energy was calculated based on 1000 snapshots taken from 1 to 6 ns MD simulation trajectories of the complex. Considering the high computational demand, only 50 snapshots evenly extracted from 1 to 6 ns were used to estimate the binding entropy.

Free Energy Decomposition Analysis. Due to the high computational demand of the PB calculations, the interaction between each residue of Aurora A and TPX2 was computed using the MM/GBSA decomposition process by the *mm/pbsa* program in AMBER9.0.⁶⁰ The essential idea of energy decomposition was to decompose the energy contribution of each residue from the association of the receptor with the ligand into three terms: van der Waals contribution (ΔE_{vdw}), electrostatic contribution (ΔE_{ele}), and solvation contribution ($\Delta G_{\text{GB}} + \Delta G_{\text{SA}}$), in which the ΔE_{vdw} and the ΔE_{ele} are van der Waals and electrostatic interactions between each residue of Aurora A and TPX2⁵¹ that could be computed by the *sander* program in AMBER9.0.⁵¹

The polar contribution of desolvation (ΔG_{GB}) was calculated using the generalized Born (GB) model, which parameters were developed by Onufriev et al.⁶¹ The nonpolar contribution of desolvation (ΔG_{SA}) was determined based on SASA determined with the ICOSA method.⁶² The residue–residue interaction spectra obtained from the MM/GBSA free energy decomposition analysis may guide us to figure out the key residues of the Aurora A/TPX2 binding. All energy components were calculated using 1000 snapshot extracted from the MD trajectory from 1 to 6 ns.

RESULTS AND DISCUSSION

Global Structure Behavior. To clarify the dynamic stability of these four complexes and to ensure the rationality of the sampling strategy, the root-mean-square-displacement (rmsd) values of the protein backbone atoms were calculated based on the starting snapshot and plotted in Figure 1. The rmsd plot indicates that the rmsd of the backbone atoms in the four complexes increases sharply within 1000 ps and then remains stable to the end of the simulation. Comparing of the rmsd average values among four systems, it could be observed that three mutants (2.3 Å, 2.2 Å, and 2.0 Å for G198N, W128F, and G198N/W128F, respectively) are less stable than that of the WT complex (1.6 Å) during the MD simulations. Additionally, from Figure S1, the potential energies of the four systems remain stable from 500 ps to the end of the simulation. According to the above analyses, it is reasonable and reliable to do the binding free energy calculation and free energy decomposition based on the snapshots extracted from 1 to 6 ns.

More detailed analyses of root-mean-square fluctuation (RMSF) versus the protein residue numbers of Aurora A and TPX2 based on the snapshots from 1 to 6 ns are illustrated in Figure 2a and 2b, respectively. It is observed that residues of Aurora A (such as Phe157, His187, Tyr199, His201, etc), which located at the interface between Aurora A and TPX2, show rigid behaviors for these four complexes. In addition, the RMSF distributions of TPX2 point out that TPX2 could form stable interactions with Aurora A at two regions (residues 8–20^{TPX2} and 31–40^{TPX2}).

Binding free Energies Predicted by MM/PBSA. To estimate the effect about W128F and G198N mutations on binding free energies, the binding affinities were calculated by the MM/PBSA method. The predicted binding affinities and the energy components of the four complexes are summarized in Table 1. As what suggested in Table 1, the predicted binding free energy of the WT complex (−137.12 kcal/mol) is more favorable than that of the G198N mutant (−114.04 kcal/mol), which is consistent with the previous report that Aurora A^{G198N} is less favorable binding to TPX2 than Aurora A^{WT}.³⁰ Besides, the binding free energy of the W128F mutant (−120.31 kcal/mol) is less favorable than that of the WT complex, showing that mutation of

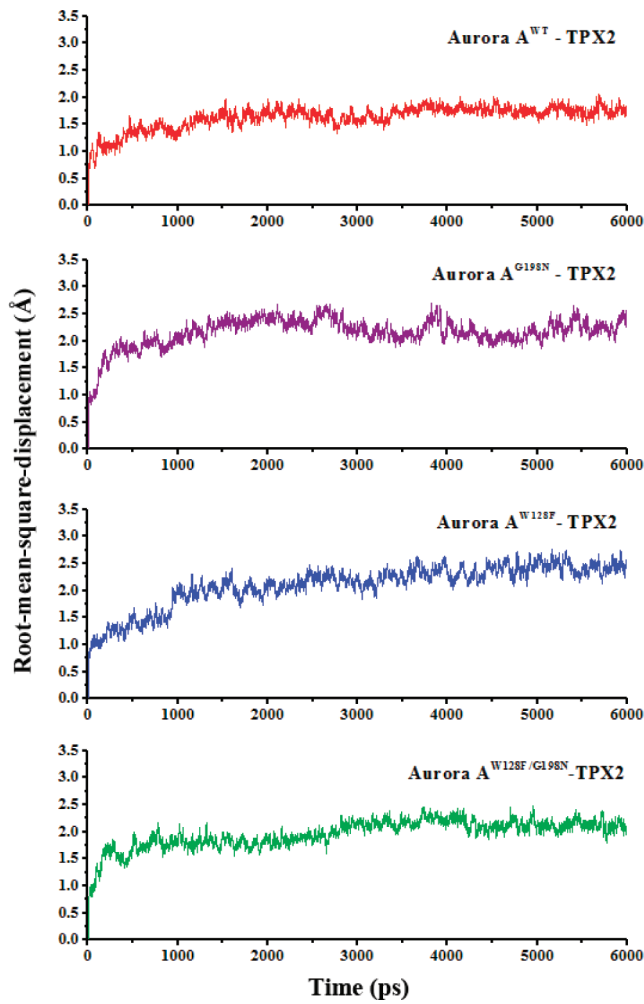


Figure 1. The root-mean-square displacements (rmsd) of the backbone atoms (CA, N, C) of the complexes with respect to the first snapshot as a function of time.

W128 in Aurora A is also unfavorable for the TPX2 binding. In addition, it is interesting to find out that the binding free energy of the G198N/W128F mutant (−123.07 kcal/mol) is more favorable than those of the two single mutants.

To get a better view on which energy term has more impact on the binding affinities, the four individual energy components (ΔE_{vdw} , ΔE_{ele} , ΔG_{PB} , and ΔG_{SA}) were carefully compared. From Table 1, it can be found that both the van der Waals (ΔE_{vdw}) and the electrostatic (ΔE_{ele}) contributions are essential for the TPX2 binding to Aurora A, in which the van der Waals interaction (ΔE_{vdw}) of the WT complex (−170.50 kcal/mol) is smaller than those of three mutants (−156.67, −157.77, and −159.06 kcal/mol for G198N, W128F, and G198N/W128F, respectively). Similarly, the electrostatic interaction (ΔE_{ele}) of WT (−1115.03 kcal/mol) is also smaller than those of the three mutants (−863.31, −944.27, and −1011.42 kcal/mol for G198N, W128F, and G198N/W128F, respectively), especially those of the two single mutants. However, considering the polar contribution of desolvation (ΔG_{PB}), which could offset the electrostatic interaction (ΔE_{ele}), the net electrostatic contributions ($\Delta E_{\text{ele}} + \Delta G_{\text{PB}}$) of the four complexes are unfavorable for the binding of Aurora A and TPX2 (58.31, 66.34, 60.53, and 59.74 kcal/mol for WT, G198N, W128F, and G198N/W128F, respectively). The nonpolar desolvation energy

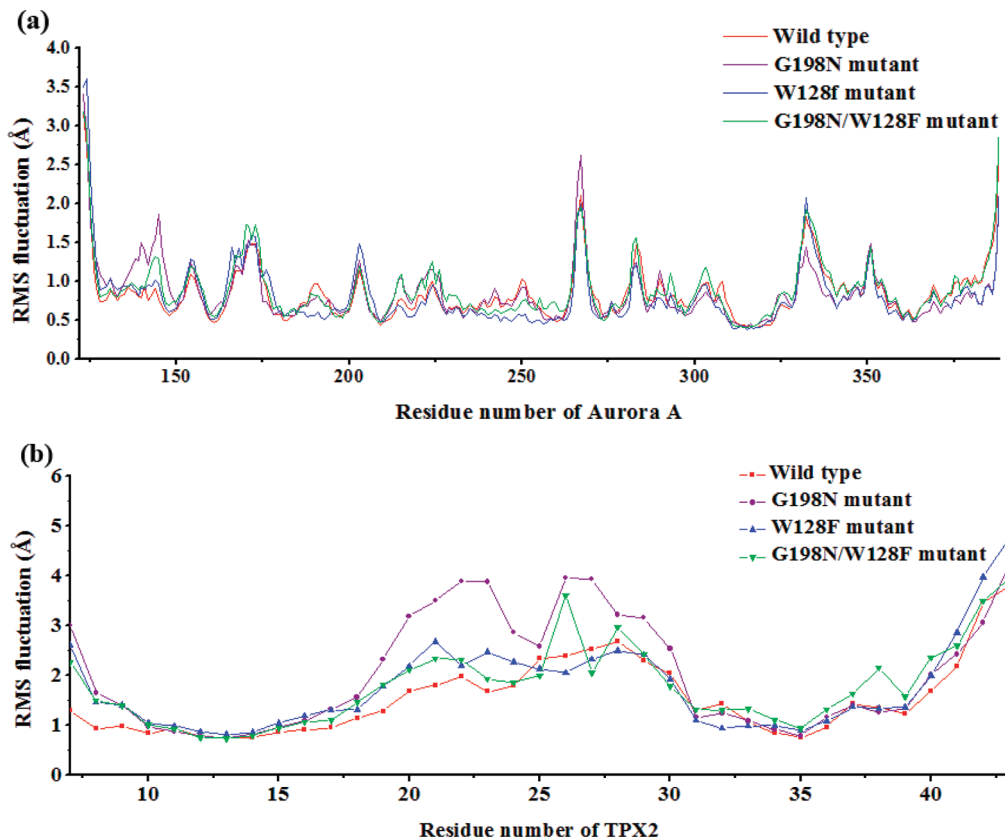


Figure 2. Root-mean-square fluctuation (RMSF) of the backbone atoms (CA, N, C) versus residue number for (a) the Aurora A and (b) the TPX2.

Table 1. Binding Free Energies and Individual Energy Terms of Aurora A with TPX2 (kcal/mol)^a

Aurora A-TPX2 complex	ΔE_{vdw}	ΔE_{ele}	ΔG_{PB}	ΔG_{SA}	$-T\Delta S$	ΔG_{pred}
Aurora A ^{WT} -TPX2	-170.50 ± 8.33	-1115.03 ± 86.89	1173.34 ± 90.93	-24.94 ± 0.99	62.87	-137.12 ± 14.57
Aurora A ^{G198N} -TPX2	-156.67 ± 9.99	-863.31 ± 83.57	929.65 ± 85.90	-23.70 ± 0.97	53.69	-114.04 ± 13.62
Aurora A ^{W128F} -TPX2	-157.77 ± 8.66	-944.27 ± 68.93	1004.80 ± 67.19	-23.09 ± 0.97	56.64	-120.31 ± 11.44
Aurora A ^{W128F/G198N} -TPX2	-159.06 ± 9.97	-1011.42 ± 83.57	1071.16 ± 87.62	-23.74 ± 1.02	57.28	-123.07 ± 14.14

^a ΔE_{vdw} , van der Waals contribution; ΔE_{ele} , electrostatic contribution; ΔG_{PB} , the polar contribution of desolvation; ΔG_{SA} , nonpolar contribution of desolvation; $-T\Delta S$, the conformational entropy at temperature T .

term (ΔG_{SA}) among these four systems are approximately the same (-24.94 , -23.70 , -23.09 , and -23.74 kcal/mol for WT, G198N, W128F, and G198N/W128F, respectively). In addition, the contributions of the conformational entropy ($-T\Delta S$) for the four complexes are 62.87, 53.69, 56.64, and 57.28 kcal/mol, respectively. Furthermore, the difference values of the van der Waals contribution among the WT complex and the three mutants are 13.83, 12.73, and 11.44 kcal/mol, while those values of the electrostatic contribution are 8.03, 2.22, and 1.43 kcal/mol. Thus, the van der Waals contribution is more crucial for distinguishing the binding affinities among these four complexes.

Binding Modes of Aurora A-TPX2 Complex. The results discussed above suggest that the mutations at residues W128 and G198 of Aurora A actually impair the binding of TPX2. To understand the influence of mutations on TPX2 binding, the binding modes of the four complexes were extensively investigated. The binding mode of the WT complex is displayed in Figure 3. It can be seen that TPX2 binds Aurora A mainly at two distinct sites on the kinase with two separated stretches. The upstream stretch of

TPX2 (residues 7–21) bind at the N-terminal of Aurora A in a mostly extended conformation. In details, the residues Tyr8^{TPX2}, Tyr10^{TPX2}, Ala12^{TPX2}, and Pro13^{TPX2} tightly nestle in a hydrophobic groove, characterized by residues His201, Val182, Tyr199, and His187 of Aurora A. Another adjacent hydrophobic pocket formed by residues Trp128^{AUR}, Phe157^{AUR}, Lys125^{AUR}, and Tyr197^{AUR} could accommodate the binding of the TPX2 residues from Phe16^{TPX2} to Phe19^{TPX2}. Particularly, the Lys125 at the N-terminal of Aurora A could form cation-π interaction with Phe19^{TPX2}.

On the other hand, the downstream stretch of TPX2 (residues 30–43) interact with Aurora A in an α-helical conformation between the N- and C-terminal lobes. The residues Trp34^{TPX2}, Phe35^{TPX2}, and Ala39^{TPX2} could bind with a hydrophobic core characterized by residues His187^{AUR}, Pro282^{AUR}, His280^{AUR}, and Leu188^{AUR}. Prominently, Trp34^{TPX2} could form strong π–π stacking interactions with His187^{AUR}, while Phe35^{TPX2} could form the T-π interactions with His280^{AUR}. Besides, an intramolecular hydrogen bond between the atom OD of Asp11^{TPX2} and

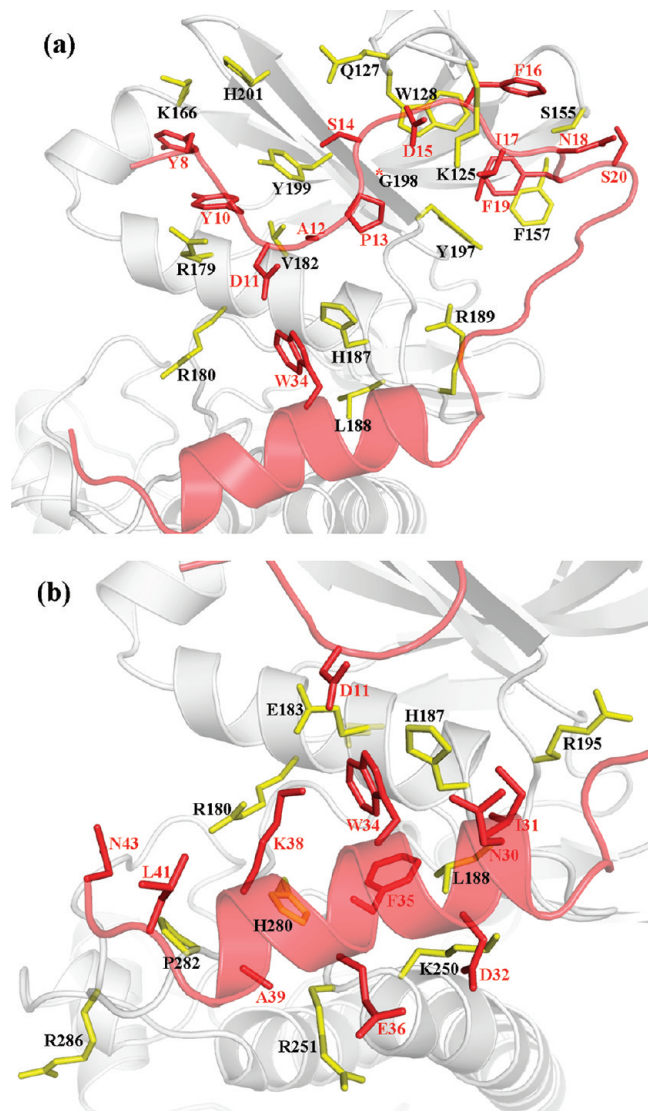


Figure 3. Binding modes of Aurora A^{WT} and TPX2 with the key residues that are essential for the binding free energy: (a) the upstream of TPX2 and (b) the downstream of TPX2.

the atom HE1 of Trp34^{TPX2} could stabilize these two binding motifs of TPX2.

Subsequently, the binding modes of two single mutants are carefully discussed and compared with that of the WT complex. For the G198N mutant illustrated in Figure 4 (the Asn198 is highlighted in red), TPX2 behaves quite differently in the binding mode with Aurora A, especially its downstream. When the glycine was mutated to the asparagine, the side chain was elongated, thus it could be in a close contact with two residues, Trp128^{AUR} and Pro13^{TPX2}. Such steric clash might result in the movement of the side chain of Trp128^{AUR} and the upstream stretch of TPX2. Due to the shift of the upstream stretch of TPX2, the residues in the flexible loop twist and thus induce the movement of the residues in the downstream stretch of TPX2. In particular, the Trp34^{TPX2} moves far away from the His187^{AUR}, thus they could not form $\pi-\pi$ stacking interactions with each other. Correspondingly, the T- π interactions between Phe35^{TPX2} and His280^{AUR} diminish.

Similarly, the binding mode of W128F mutant (Figure S2) also changes. When the indole ring of W was substituted by the

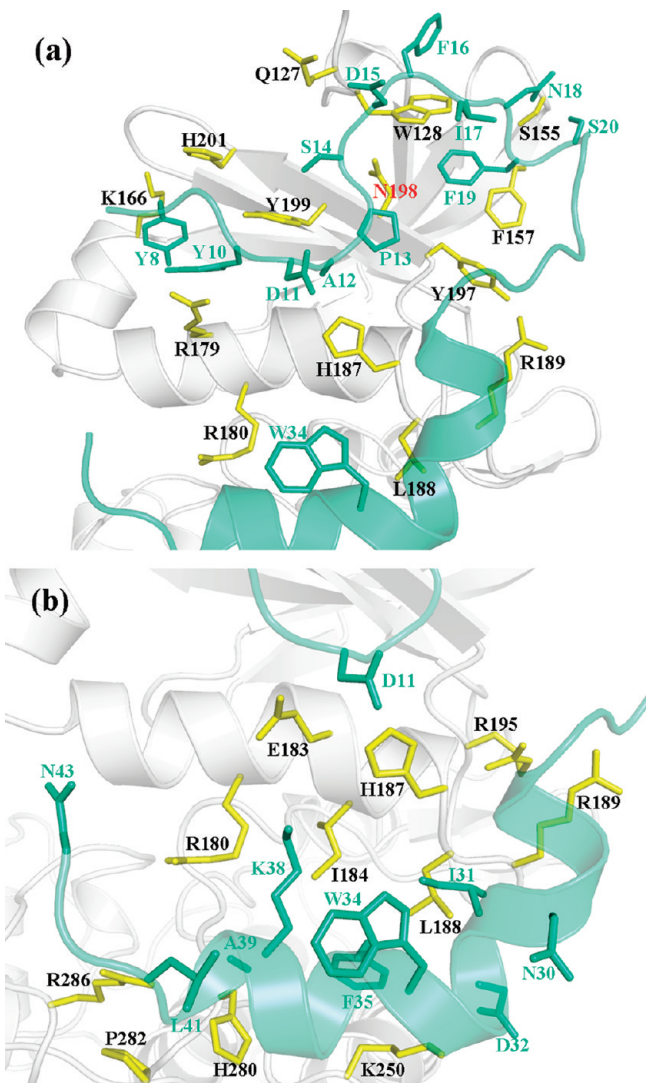


Figure 4. Binding modes of Aurora A^{G198N} and TPX2 with the key residues that are essential for the binding free energy: (a) the upstream of TPX2 and (b) the downstream of TPX2.

phenyl ring of F, the side chain was shortened, and thus drive the hydrophobic residues (such as Phe16^{TPX2}, Ile17^{TPX2}, and Phe19^{TPX2}) surrounding F128 move forward to this residue. This movement leads to the shift of the residues in the upstream stretch and in the flexible loop of TPX2 and further affects the stability of the downstream of TPX2. In special, the Tyr8^{TPX2} could not form $\pi-\pi$ stacking interactions with His201^{AUR} but have a cation- π interaction with Arg179^{AUR}.

To further discuss the cooperative effect of these two amino acids on Aurora A and TPX2 binding, the double mutant (G198N/W128F, Figure S3) was studied. In this mutant, both the small and large residues (G and W) were substituted by the medium sized residues (N and F), so the variations surrounding these two amino acids might diminish, which could interpret the reason that the predicted binding free energy of this mutant is more favorable than those of the two single mutants. Despite the movements surrounding these two residues reduce, they still drive the twist of the residues in the flexible loop of TPX2 and affect the α -helical conformation of the downstream of TPX2.

Table 2. Visible Percentage of Hydrogen Bonds during MD Simulations between Aurora A and TPX2

complex	donor	acceptor	occupied (%)	distance (Å)	angle (deg)
Aurora A ^{WT} -TPX2	:126@O	:16@H-16@N (TPX2)	99.77	2.958	162.44
	:183@OE	:11@H-11@N (TPX2)	99.45	2.958	165.06
	:8@O (TPX2)	:199@HH-199@OH	95.47	2.809	154.76
	:14@O (TPX2)	:128@H-128@N	94.78	3.071	156.32
	:24@OD (TPX2)	:189@HE-189@NE	94.07	2.969	150.79
	:175@OE	:7@H-7@N (TPX2)	81.50	2.883	146.78
	:13@O (TPX2)	:199@H-199@N	75.12	3.150	150.88
	:199@OH	:10@H-10@N (TPX2)	59.48	3.016	149.03
	:11@O (TPX2)	:187@HE2-187@NE2	47.73	3.049	152.72
	:43@OXT (TPX2)	:284@HG-284@OG	39.43	2.632	165.25
	:39@O (TPX2)	:283@HG-283@OG	32.32	2.84	151.62
	:284@OG	:43@H-43@N (TPX2)	30.70	3.138	147.88
	:35@O (TPX2)	:280@HE2-280@NE2	29.65	3.047	134.79
	:15@O (TPX2)	:128@HE1-128@NE1	27.08	2.957	130.44
	:11@OD (TPX2)	:187@HE2-187@NE2	22.77	3.020	142.95
	:183@OE	:11@H-11@N (TPX2)	97.57	2.917	165.09
	:126@O	:16@H-16@N (TPX2)	86.68	3.025	153.22
Aurora A ^{G198N} -TPX2	:13@O (TPX2)	:199@H-199@N	85.02	3.111	152.97
	:8@O (TPX2)	:199@HH-199@OH	72.55	2.868	146.48
	:199@OH	:10@H-10@N (TPX2)	49.87	3.131	148.93
	:11@O (TPX2)	:187@HE2-187@NE2	43.65	3.025	146.83
	:175@OE	:7@H-7@N (TPX2)	42.75	2.938	144.99
	:15@O (TPX2)	:128@HE1-128@NE1	37.60	3.030	138.38
	:183@OE	:11@H-11@N (TPX2)	99.03	2.873	164.77
	:126@O	:16@H-16@N (TPX2)	93.87	3.016	161.38
	:13@O (TPX2)	:199@H-199@N	89.15	3.047	152.73
	:14@O (TPX2)	:128@H-128@N	84.97	3.050	156.33
Aurora A ^{W128F} -TPX2	:24@OD (TPX2)	:189@HE-189@NE	62.17	3.046	152.46
	:199@OH	:10@H-10@N (TPX2)	58.17	3.186	156.32
	:8@O (TPX2)	:199@HH-199@OH	48.85	2.848	149.21
	:11@O (TPX2)	:187@HE2-187@NE2	35.92	3.039	142.83
	:175@OE	:7@H-7@N (TPX2)	34.74	2.858	150.32
	:11@OD (TPX2)	:187@HE2-187@NE2	23.77	2.998	143.53
	:8@O (TPX2)	:199@HH-199@OH	94.27	2.800	152.21
	:183@OE	:11@H-11@N (TPX2)	90.46	2.897	163.66
	:199@OH	:10@H-10@N (TPX2)	77.50	3.034	150.70
	:126@O	:16@H-16@N (TPX2)	68.43	2.977	161.20
Aurora A ^{G198N/W128F} -TPX2	:13@O (TPX2)	:199@H-199@N	67.00	3.119	153.02
	:14@O (TPX2)	:128@H-128@N	60.92	3.040	157.66
	:175@OE	:7@H-7@N (TPX2)	51.38	2.885	149.89
	:35@O (TPX2)	:280@HE2-280@NE2	43.98	2.990	143.92
	:43@OXT (TPX2)	:284@HG-284@OG	39.60	2.629	163.58
	:284@OG	:43@H-43@N (TPX2)	32.07	3.109	151.59
	:11@OD (TPX2)	:187@HE2-187@NE2	30.37	2.967	149.63

Moreover, in order to investigate the influence of the mutation on the hydrogen bonding network, the visible percentage of hydrogen bonds between Aurora A and TPX2 during the MD simulations was calculated, and the results were summarized in Table 2. In the hydrogen bond calculation, a hydrogen bond was defined if the donor–acceptor(H) distance was smaller than 3.2 Å and the donor–acceptor(H)-acceptor angle was larger than 120°. Besides, the angles listed in Table 2 are the real hydrogen bond angles rather than the stored angles obtained from the *ptra*j

program of AMBER (the stored angles are the supplementary angles of the real hydrogen bond angles). Clearly, both the single and double mutations lead to some variant hydrogen bonding interactions between the Aurora A and TPX2. The number of the hydrogen bond of the WT complex is more than those of the three mutants, which is inconsistent with the results of the electrostatic interactions discussed above.

The Stability of TPX2. The comparison between the WT complex and the G198N mutant (as illustrated in Figure 5)

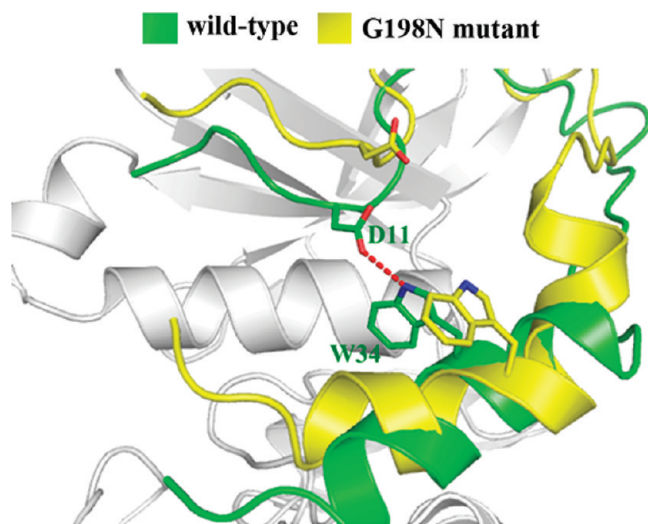


Figure 5. The comparison of the structure for TPX2 between the WT complex and the G198N mutant.

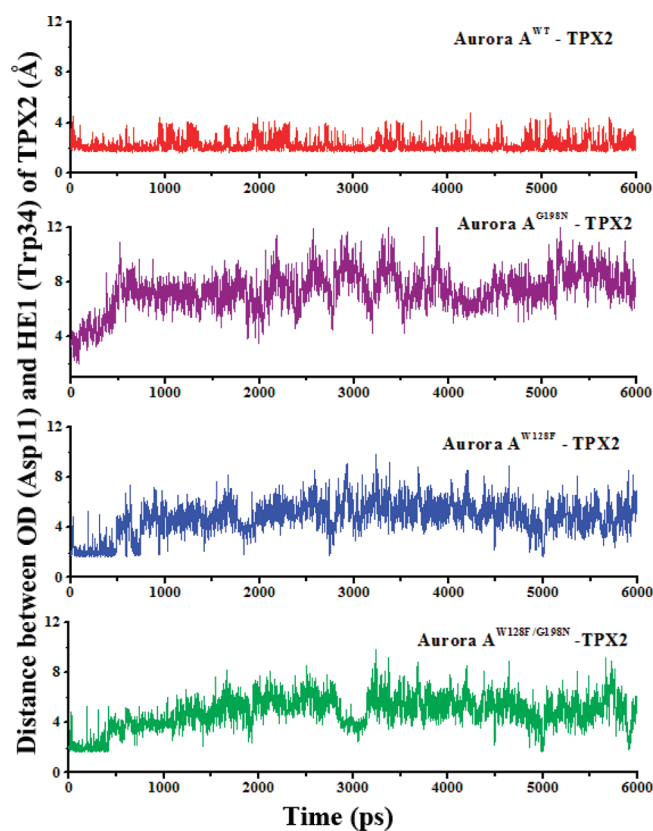


Figure 6. The distance between atom OD (Asp11) and NE1 (Trp34) of TPX2 during MD simulation.

displays the large structural changes of TPX2. Obviously, for the G198N mutant, the intramolecular hydrogen bond between the atom OD of Asp11^{TPX2} and the atom HE1 of Trp34^{TPX2} disappear and thus break down the stability of the secondary structure of TPX2. To quantify the effects of mutation on the stability of TPX2, the distance between these two atoms for the four complexes during the MD simulations was calculated and plotted in Figure 6. Evidently, the distance of the WT complex fluctuates

around 2.5 Å during the MD simulation. Further analysis of the hydrogen bond occupancy between these two atoms of the WT complex based on the snapshots from 1 to 6 ns is 80.74, demonstrating that this hydrogen bond is quite stable during the MD simulation. However, for the three mutants, the distances between these two atoms are larger than 5 Å, which is not suitable for the hydrogen bond formation. This result indicates that the mutations break down the stability of TPX2 and thus affect the recognition between Aurora A and TPX2.

Decomposition Analysis of the Binding Free Energies. As stated above, the mutations at residues W128 and G198 of Aurora A alter the binding pattern between Aurora A and TPX2 compared to the wild-type complex. To further understand the detailed presentation of the Aurora A/TPX2 interactions, MM/GBSA free energy decomposition analysis was employed to decompose the total binding free energies into residue–residue pairs, which would provide more quantitative analysis information of each residue's contribution.

The comparison of the key contributors of Aurora A for the four complexes is shown in Figure 7. Compared with the WT complex and the G198N mutant, it can be observed that the distinct difference between them could be mainly identified on five residues, Lys125, Trp128, His187, Gly198, and Pro282. Among them, the interactions between TPX2 and residues Lys125, Trp128, His187, and Pro282 of the WT complex (−4.19, −6.86, −5.29, and −2.46 kcal/mol) are more favorable than those of the G198N mutant (−2.94, −5.92, −3.62, and −1.45 kcal/mol). But, the interaction of TPX2 with residue Gly198 of the WT complex (−1.36 kcal/mol) is less favorable than that of the residue Asn198 of the G198N mutant (−2.79 kcal/mol), which might be explained by the reason that the side chain of Asn198 could have strong interactions with the surrounding residues. For the W128F mutant, five residues (Lys125, Trp128, Lys166, His187, and His201) of Aurora A, which interact with TPX2 (−1.89, −5.49, −0.25, −4.02, and −0.24 kcal/mol) are less favorable than those of the WT complex (−4.19, −6.86, −1.48, −5.29, and −1.54 kcal/mol), were determined to play crucial roles in distinguishing the binding modes. Among them, when the Trp128 was substituent by the Phe128, the side chain of this residue lessens and thus the van der Waals interactions with TPX2 might diminish, which is in accordance with the contribution of this residue increased from −6.86 to −5.49 kcal/mol. Because the Tyr8^{TPX2} in the W128F mutant moves far away from the His201^{AUR}, they could not form the π–π stacking interactions with each other, which could interpret that the contribution of His201 increased from −1.54 to −0.24 kcal/mol. Besides, the comparison between the G198N/W128F mutant and the WT complex illustrates that the dominating difference between them could attribute to four residues of Aurora A, Gln127, Trp128, His187, and Gly198. Of all these residues, except residue Gly198, the interactions between TPX2 and other three residues (Gln127, Trp128, and His187) of the G198N/W128F mutant (−2.41, −3.97, and −4.08 kcal/mol) are less favorable than those of the WT complex (−3.72, −6.86, and −5.29 kcal/mol).

In addition, the residue–residue interaction spectra of TPX2 for the four complexes were plotted in Figure 8. It can be seen most of the residues in the upstream of TPX2 of the four complexes (such as Tyr8, Tyr10, Phe16, and Phe19) have similar binding patterns with Aurora A, which is in accordance with the discussion about the interaction modes of Aurora A and the upstream strength of TPX2. However, a distinct difference could be found on two conserved aromatic residues in the downstream

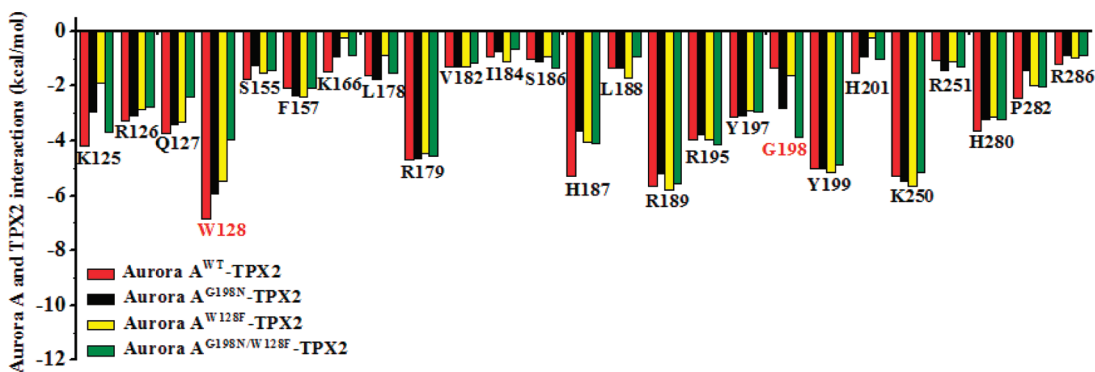


Figure 7. The comparison of key contributors of Aurora A for four complexes.

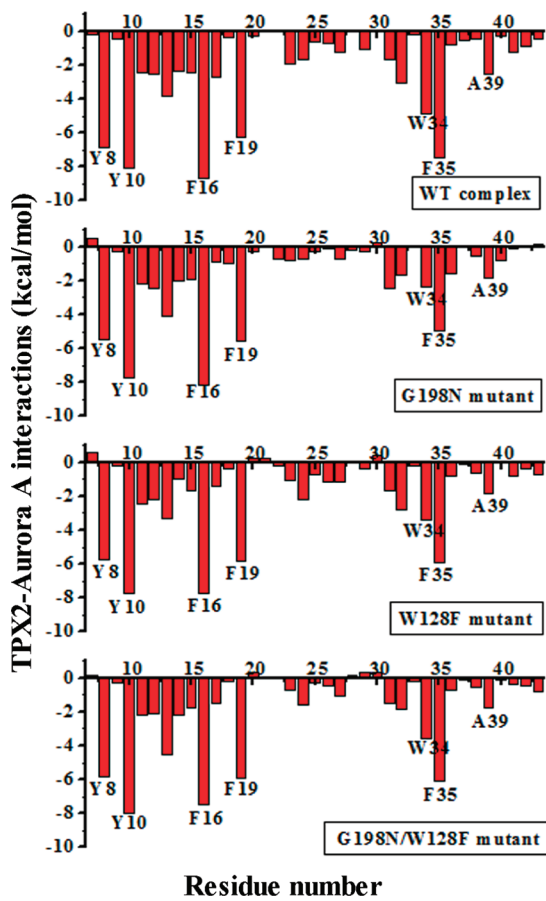


Figure 8. The residue–residue interaction spectrum of TPX2 for four complexes.

of TPX2 (Trp34 and Phe35). Compared with the WT complex and the G198N mutant, it is notable that the interaction between Aurora A and these two residues of the WT complex (-4.83 and -7.45 kcal/mol) are more favorable than those of the G198N mutant (-2.33 and -4.95 kcal/mol), which could be explained by the fact that the movement of the residues in the downstream of TPX2 diminish the binding strength with Aurora A. Similarly, the contribution of these two residues in the W128F mutant (-3.42 and -5.89 kcal/mol) and the G198N/W128F mutant (-3.57 and -6.11 kcal/mol) are also less favorable than the WT complex. The results demonstrate that the mutations at residues W128 and G198 of Aurora A actually convert the binding modes

between Aurora A and TPX2, especially the downstream of TPX2.

CONCLUSION

In the present study, to clarify the structural effect of mutations for G198N and W128F influence the binding modes between Aurora A and TPX2, MD simulations, MM/PBSA free energy calculations, and MM/GBSA free energy decomposition analysis were conducted. The calculating results show that the predicted binding free energy of the WT complex is more favorable than that of the G198N mutant, which is in accordance with the experimental data. Similarly, the binding free energies of the other two mutants are less favorable than that of the WT complex, indicating both single and double mutations of these two amino acids are unfavorable for the Aurora A and TPX2 binding. The analysis of individual energy terms demonstrated that both the van der Waals and electrostatic contribution are essential for the Aurora A and TPX2 binding. It is also observed that the van der Waals contribution is more crucial for distinguishing the binding affinities among these four complexes.

According to the structural analysis, the mutations at residues W128 and G198 of Aurora A alter the binding pattern between Aurora A and TPX2, especially the downstream of TPX2. In the G198N mutant, the steric clash surrounding asparagine leads to the movement of the upstream stretch of TPX2 and thus drives the shift of the residues in downstream stretch of TPX2. For W128F mutant, the shortened side chain induces the hydrophobic residues encircling F128 move forward to this residues and further affects the stability of the downstream of TPX2. But for the G198N/W128F mutant, though the variations surrounding these two residues diminish, it still induces the variation of the conformation of the downstream of TPX2. The analysis of hydrogen bond occupancy between Aurora A and TPX2 manifest that the number of the hydrogen bonds of the WT complex is more than those of the three mutants, resulting in the variant electrostatic contributions. The analysis also indicates an intramolecular hydrogen bond between the atom OD of Asp $^{11}_{\text{TPX2}}$ and the atom HE1 of Trp $^{34}_{\text{TPX2}}$, which is responsible for the stability of TPX2, disappears in three mutants. Moreover, based on the free energy decomposition analysis, the difference of the binding free energy is primarily determined by two residues (Trp34 and Phe35) of TPX2. In summary, it is feasible to investigate the mutation effect on the protein–protein binding via the combination of different molecular modeling techniques. We hope this work would provide a possible structural explanation for the understanding of specific binding between Aurora A and TPX2 as well as give

valuable information for the future design of specific peptide inhibitors for Aurora A.

■ ASSOCIATED CONTENT

S Supporting Information. Figure S1: The potential energies of four complexes with respect to the first snapshot as a function of time. Figure S2: Binding mode of Aurora A^{W128F} and TPX2 with the key residues that are essential for the binding free energy. Figure S3: Binding mode of Aurora A^{G198N/W128F} and TPX2 with the key residues that are essential for the binding free energy. This material is available free of charge via the Internet at <http://pubs.acs.org>.

■ AUTHOR INFORMATION

Corresponding Author

*Phone: +86 10 88256326. Fax: +86 10 88256093. E-mail: jmj@gucas.ac.cn (M.J.). Phone: +86 10 82543578. E-mail: chtung@mail.ipc.ac.cn (C.-H.T.).

■ ACKNOWLEDGMENT

The project was supported by the National Science and Technology Major Special Project of China (No. 2009ZX09501-011) and the Natural Science Foundation of China (No. 21073105 and No. 21173264).

■ REFERENCES

- (1) Bischoff, J. R.; Plowman, G. D. The Aurora/Ipl1p Kinase Family: Regulators of Chromosome Segregation and Cytokinesis. *Trends Cell Biol.* **1999**, *9*, 454–459.
- (2) Meraldi, P.; Honda, R.; Nigg, E. A. Aurora Kinases Link Chromosome Segregation and Cell Division to Cancer Susceptibility. *Curr. Opin. Genet. Dev.* **2004**, *14*, 29–36.
- (3) Keen, N.; Taylor, S. Aurora-Kinase Inhibitors as Anticancer Agents. *Nat. Rev. Cancer* **2004**, *4*, 927–936.
- (4) Katayama, H.; Brinkley, W. R.; Sen, S. The Aurora Kinases: Role in Cell Transformation and Tumorigenesis. *Cancer Metastasis Rev.* **2003**, *22*, 451–464.
- (5) Fu, J.; Bian, M.; Jiang, Q.; Zhang, C. Roles of Aurora Kinases in Mitosis and Tumorigenesis. *Mol. Cancer Res.* **2007**, *5*, 1–10.
- (6) Andrews, P. D. Aurora Kinases: Shining Lights on the Therapeutic Horizon? *Oncogene* **2005**, *24*, 5005–5015.
- (7) Carmena, M.; Earnshaw, W. C. The Cellular Geography of Aurora Kinases. *Nat. Rev. Mol. Cell Biol.* **2003**, *4*, 842–854.
- (8) Marumoto, T.; Zhang, D.; Saya, H. Aurora-A - A Guardian of Poles. *Nat. Rev. Cancer* **2005**, *5*, 42–50.
- (9) Dutertre, S.; Descamps, S.; Prigent, C. On the Role of Aurora-A in Centrosome Function. *Oncogene* **2002**, *21*, 6175–6183.
- (10) Barr, A. R.; Gergely, F. Aurora-A: the Maker and Breaker of Spindle Poles. *J. Cell. Sci.* **2007**, *120*, 2987–2996.
- (11) Yang, H.; Ou, C. C.; Feldman, R. I.; Nicosia, S. V.; Kruk, P. A.; Cheng, J. Q. Aurora-A Kinase Regulates Telomerase Activity through c-Myc in Human Ovarian and Breast Epithelial Cells. *Cancer Res.* **2004**, *64*, 463–467.
- (12) Zhou, H.; Kuang, J.; Zhong, L.; Kuo, W.-l.; Gray, J.; Sahin, A.; Brinkley, B.; Sen, S. Tumour Amplified Kinase STK15/BTAK Induces Centrosome Amplification, Aneuploidy and Transformation. *Nat. Genet.* **1998**, *20*, 189–193.
- (13) Murata-Hori, M.; Wang, Y.-l. The Kinase Activity of Aurora B Is Required for Kinetochore-Microtubule Interactions during Mitosis. *Curr. Biol.* **2002**, *12*, 894–899.
- (14) Adams, R. R.; Maiato, H.; Earnshaw, W. C.; Carmena, M. Essential Roles of Drosophila Inner Centromere Protein (Incenp) and Aurora B in Histone H3 Phosphorylation, Metaphase Chromosome Alignment, Kinetochore Disjunction, and Chromosome Segregation. *J. Cell Biol.* **2001**, *153*, 865–880.
- (15) Biggins, S.; Murray, A. W. The Budding Yeast Protein Kinase Ipl1/Aurora Allows the Absence of Tension to Activate the Spindle Checkpoint. *Genes Dev.* **2001**, *15*, 3118–3129.
- (16) Ditchfield, C.; Johnson, V. L.; Tighe, A.; Ellston, R.; Haworth, C.; Johnson, T.; Mortlock, A.; Keen, N.; Taylor, S. S. Aurora B Couples Chromosome Alignment with Anaphase by Targeting BubR1, Mad2, and Cenp-E to Kinetochore. *J. Cell Biol.* **2003**, *161*, 267–280.
- (17) Kufer, T. A.; Sillje, H. H. W.; Körner, R.; Gruss, O. J.; Meraldi, P.; Nigg, E. A. Human TPX2 Is Required for Targeting Aurora-A Kinase to the Spindle. *J. Cell Biol.* **2002**, *158*, 617–623.
- (18) Ozlü, N.; Srayko, M.; Kinoshita, K.; Habermann, B.; O Toole, E. T.; Müller-Reichert, T.; Schmalz, N.; Desai, A.; Hyman, A. A. An Essential Function of the *C. elegans* Ortholog of TPX2 Is to Localize Activated Aurora A Kinase to Mitotic Spindles. *Dev. Cell* **2005**, *9*, 237–248.
- (19) Bayliss, R.; Sardon, T.; Vernos, I.; Conti, E. Structural Basis of Aurora-A Activation by TPX2 at the Mitotic Spindle. *Mol. Cell* **2003**, *12*, 851–862.
- (20) Eyers, P. A.; Maller, J. L. Regulation of Xenopus Aurora A Activation by TPX2. *J. Biol. Chem.* **2004**, *279*, 9008–9015.
- (21) Eyers, P. A.; Erikson, E.; Chen, L. G.; Maller, J. L. A Novel Mechanism for Activation of the Protein Kinase Aurora A. *Curr. Biol.* **2003**, *13*, 691–697.
- (22) Ferchichi, I.; Stambouli, N.; Marrackchi, R.; Arlot, Y.; Prigent, C.; Fadiel, A.; Odunsi, K.; Ben Ammar Elgaaied, A.; Hamza, A. Experimental and Computational Studies Indicate Specific Binding of pVHL Protein to Aurora-A Kinase. *J. Phys. Chem. B* **2010**, *114*, 1486–1497.
- (23) Kaitna, S.; Mendoza, M.; Jantsch-Plunger, V.; Glotzer, M. Incenp and an Aurora-Like Kinase Form a Complex Essential for Chromosome Segregation and Efficient Completion of Cytokinesis. *C* **2000**, *10*, 1172–1181.
- (24) Adams, R. R.; Wheatley, S. P.; Gouldsworth, A. M.; Kandels-Lewis, S. E.; Carmena, M.; Smythe, C.; Gerloff, D. L.; Earnshaw, W. C. INCENP Binds the Aurora-Related Kinase AIRK2 and Is Required to Target it to Chromosomes, the Central Spindle and Cleavage Furrow. *Curr. Biol.* **2000**, *10*, 1075–1078.
- (25) Wheatley, S. P.; Carvalho, A.; Vagnarelli, P.; Earnshaw, W. C. INCENP Is Required for Proper Targeting of Survivin to the Centromeres and the Anaphase Spindle During Mitosis. *Curr. Biol.* **2001**, *11*, 886–890.
- (26) Bolton, M. A.; Lan, W.; Powers, S. E.; McCleland, M. L.; Kuang, J.; Stukenberg, P. T. Aurora B Kinase Exists in a Complex with Survivin and INCENP and Its Kinase Activity Is Stimulated by Survivin Binding and Phosphorylation. *Mol. Biol. Cell* **2002**, *13*, 3064–3077.
- (27) Sampath, S. C.; Ohi, R.; Leismann, O.; Salic, A.; Pozniakowski, A.; Funabiki, H. The Chromosomal Passenger Complex Is Required for Chromatin-Induced Microtubule Stabilization and Spindle Assembly. *Cell* **2004**, *118*, 187–202.
- (28) Sessa, F.; Mapelli, M.; Ciferri, C.; Tarricone, C.; Areces, L. B.; Schneider, T. R.; Stukenberg, P. T.; Musacchio, A. Mechanism of Aurora B Activation by INCENP and Inhibition by Hesperadin. *Mol. Cell* **2005**, *18*, 379–391.
- (29) Bayliss, R.; Sarfon, T.; Ebert, J.; Lindner, D.; Vernos, I.; Conti, E. Determinants for Aurora-A Activation and Aurora-B Discrimination by TPX2. *Cell Cycle* **2004**, *3*, 404–407.
- (30) Eyers, P. A.; Churchill, M. E. A.; Maller, J. L. The Aurora A and Aurora B Protein Kinases A single Amino Acid Difference Controls Intrinsic Activity and Activation by TPX2. *Cell Cycle* **2005**, *4*, 784–789.
- (31) Fu, J.; Bian, M.; Liu, J.; Jiang, Q.; Zhang, C. A Single Amino Acid Change Converts Aurora-A into Aurora-B-Like Kinase in Terms of Partner Specificity and Cellular Function. *Proc. Natl. Acad. Sci. USA* **2009**, *106*, 6939–6944.
- (32) Wang, W.; Kollman, P. A. Free Energy Calculations on Dimer Stability of the HIV Protease using Molecular Dynamics and a Continuum Solvent Model. *J. Mol. Biol.* **2000**, *303*, 567–582.
- (33) Matthew, R. L.; Yong, D.; Peter, A. K. Use of MM-PB/SA in Estimating the Free Energies of Proteins: Application to Native, Intermediates, and Unfolded Villin Headpiece. *Proteins* **2000**, *39*, 309–316.

- (34) Kuhn, B.; Kollman, P. A. Binding of a Diverse Set of Ligands to Avidin and Streptavidin: An Accurate Quantitative Prediction of Their Relative Affinities by a Combination of Molecular Mechanics and Continuum Solvent Models. *J. Med. Chem.* **2000**, *43*, 3786–3791.
- (35) Kollman, P. A.; Massova, I.; Reyes, C.; Kuhn, B.; Huo, S.; Chong, L.; Lee, M.; Lee, T.; Duan, Y.; Wang, W.; Donini, O.; Cieplak, P.; Srinivasan, J.; Case, D. A.; Cheatham, T. E. Calculating Structures and Free Energies of Complex Molecules: Combining Molecular Mechanics and Continuum Models. *Acc. Chem. Res.* **2000**, *33*, 889–897.
- (36) Hou, T.; Guo, S.; Xu, X. Predictions of Binding of a Diverse Set of Ligands to Gelatinase-A by a Combination of Molecular Dynamics and Continuum Solvent Models. *J. Phys. Chem. B* **2002**, *106*, 5527–5535.
- (37) Hou, T.; Zhu, L.; Chen, L.; Xu, X. Mapping the Binding Site of a Large Set of Quinazoline Type EGF-R Inhibitors Using Molecular Field Analyses and Molecular Docking Studies. *J. Chem. Inf. Comput. Sci.* **2002**, *43*, 273–287.
- (38) Wang, J.; Morin, P.; Wang, W.; Kollman, P. A. Use of MM-PBSA in Reproducing the Binding Free Energies to HIV-1 RT of TIBO Derivatives and Predicting the Binding Mode to HIV-1 RT of Efavirenz by Docking and MM-PBSA. *J. Am. Chem. Soc.* **2001**, *123*, 5221–5230.
- (39) Wang, W.; Kollman, P. A. Computational Study of Protein Specificity: The Molecular Basis of HIV-1 Protease Drug Resistance. *Proc. Natl. Acad. Sci. USA* **2001**, *98*, 14937–14942.
- (40) Lepšík, M.; Kríž, Z.; Havlas, Z. Efficiency of a Second-Generation HIV-1 Protease Inhibitor Studied by Molecular Dynamics and Absolute Binding Free Energy Calculations. *Proteins* **2004**, *57*, 279–293.
- (41) Hou, T.; Chen, K.; McLaughlin, W. A.; Lu, B.; Wang, W. Computational Analysis and Prediction of the Binding Motif and Protein Interacting Partners of the Abl SH3 Domain. *PLoS Comput. Biol.* **2006**, *2*, 47–56.
- (42) Weis, A.; Katebzadeh, K.; Söderhjelm, P.; Nilsson, I.; Ryde, U. Ligand Affinities Predicted with the MM/PBSA Method: Dependence on the Simulation Method and the Force Field. *J. Med. Chem.* **2006**, *49*, 6596–6606.
- (43) Hou, T.; Yu, R. Molecular Dynamics and Free Energy Studies on the Wild-type and Double Mutant HIV-1 Protease Complexed with Amprenavir and Two Amprenavir-Related Inhibitors: Mechanism for Binding and Drug Resistance. *J. Med. Chem.* **2007**, *50*, 1177–1188.
- (44) Luo, R.; David, L.; Gilson, M. K. Accelerated Poisson–Boltzmann calculations for static and dynamic systems. *J. Comput. Chem.* **2002**, *23*, 1244–1253.
- (45) Hou, T.; Wang, J.; Li, Y.; Wang, W. Assessing the Performance of the MM/PBSA and MM/GBSA Methods. 1. The Accuracy of Binding Free Energy Calculations Based on Molecular Dynamics Simulations. *J. Chem. Inf. Model.* **2011**, *51*, 69–82.
- (46) Holger, G.; David, A. C. Converging Free Energy Estimates: MM-PB(GB)SA Studies on the Protein-Protein Complex Ras-Raf. *J. Comput. Chem.* **2004**, *25*, 238–250.
- (47) Hou, T.; McLaughlin, W.; Lu, B.; Chen, K.; Wang, W. Prediction of Binding Affinities between the Human Amphiphysin-1 SH3 Domain and Its Peptide Ligands Using Homology Modeling, Molecular Dynamics and Molecular Field Analysis. *J. Prote. Res.* **2005**, *5*, 32–43.
- (48) Hou, T.; Zhang, W.; Case, D. A.; Wang, W. Characterization of Domain-Peptide Interaction Interface: A Case Study on the Amphiphysin-1 SH3 Domain. *J. Mol. Biol.* **2008**, *376*, 1201–1214.
- (49) Fang, L.; Zhang, H.; Cui, W.; Ji, M. Studies of the Mechanism of Selectivity of Protein Tyrosine Phosphatase 1B (PTP1B) Bidentate Inhibitors Using Molecular Dynamics Simulations and Free Energy Calculations. *J. Chem. Inf. Model.* **2008**, *48*, 2030–2041.
- (50) Berman, H. M.; Westbrook, J.; Feng, Z.; Gilliland, G.; Bhat, T. N.; Weissig, H.; Shindyalov, I. N.; Bourne, P. E. The Protein Data Bank. *Nucleic Acids Res.* **2000**, *28*, 235–242.
- (51) David, A. C.; Thomas, E. C., III; Tom, D.; Holger, G.; Ray, L.; Kenneth, M. M., Jr.; Alexey, O.; Carlos, S.; Bing, W.; Robert, J. W. The Amber Biomolecular Simulation Programs. *J. Comput. Chem.* **2005**, *26*, 1668–1688.
- (52) Yong, D.; Chun, W.; Shbasish, C.; Mathew, C. L.; Guoming, X.; Wei, Z.; Rong, Y.; Piotr, C.; Ray, L.; Taisung, L.; James, C.; Junmei, W.; Peter, K. A Point-Charge Force Field for Molecular Mechanics Simulations of Proteins Based on Condensed-Phase Quantum Mechanical Calculations. *J. Comput. Chem.* **2003**, *24*, 1999–2012.
- (53) Craft, J.; Legge, G. An AMBER/DYANA/MOLMOL Phosphorylated Amino Acid Library Set and Incorporation into NMR Structure Calculations. *J. Biomol. NMR* **2005**, *33*, 15–24.
- (54) Meagher, K. L.; Redman, L. T.; Carlson, H. A. Development of Polyphosphate Parameters for Use with the AMBER Force Field. *J. Comput. Chem.* **2003**, *24*, 1016–1025.
- (55) William, L. J.; Jayaraman, C.; Jeffry, D. M.; Roger, W. I.; Michael, L. K. Comparison of Simple Potential Functions for Simulating Liquid Water. *J. Chem. Phys.* **1983**, *79*, 926–935.
- (56) Tom, D.; Darrin, Y.; Lee, P. Particle mesh Ewald: An N [center-dot] log(N) Method for Ewald Sums in Large Systems. *J. Chem. Phys.* **1993**, *98*, 10089–10092.
- (57) Ryckaert, J.-P.; Ciccotti, G.; Berendsen, H. J. C. Numerical Integration of the Cartesian Equations of Motion of a System with Constraints: Molecular Dynamics of n-Alkanes. *J. Comput. Phys.* **1977**, *23*, 327–341.
- (58) Gilson, M. K.; Sharp, K. A.; Honig, B. H. Calculating the Electrostatic Potential of Molecules in Solution: Method and Error Assessment. *J. Comput. Chem.* **1988**, *9*, 327–335.
- (59) Jörg, W.; Peter, S. S.; Still, W. C. Approximate Atomic Surfaces from Linear Combinations of Pairwise Overlaps (LCPO). *J. Comput. Chem.* **1999**, *20*, 217–230.
- (60) Gohlke, H.; Kiel, C.; Case, D. A. Insights into Protein-Protein Binding by Binding Free Energy Calculation and Free Energy Decomposition for the Ras-Raf and Ras-RalGDS Complexes. *J. Mol. Biol.* **2003**, *330*, 891–913.
- (61) Alexey, O.; Donald, B.; David, A. C. Exploring Protein Native States and Large-Scale Conformational Changes with a Modified Generalized Born Model. *Proteins* **2004**, *55*, 383–394.
- (62) Case, D. A.; Darden, T. A.; Cheatham; Simmerling, C. L.; Wang, J.; Duke, R. E.; Luo, R.; Merz, K. M.; Pearlman, D. A.; Crowley, M.; Walker, R. C.; Zhang, W.; Wang, B.; Hayik, S.; Roitberg, A.; Seabra, G.; Wong, K. F.; Paesani, F.; Wu, X.; Brozell, S.; Tsui, V.; Gohlke, H.; Yang, L.; Tan, C.; Mongan, J.; Hornak, V.; Cui, G.; Beroza, P.; Mathews, D. H.; Schafmeister, C.; Ross, W. S.; Kollman, P. A. *Amber* 9. 2006.